

## Original Article

# Investigation into the mechanistic action of zhuye shigao decoction in acute pneumonia treatment via liquid chromatography-mass spectrometry-based metabolomics combined with network pharmacology analysis

Zhiliang Sun<sup>†,a</sup>, Haipeng Tang<sup>†,a</sup>, Guangzhi Cai<sup>a</sup>, Kejin Xu<sup>a</sup>, Yang Wang<sup>b,\*</sup>, Jiyu Gong<sup>a</sup>

<sup>a</sup>School of Pharmaceutical Sciences, Changchun University of Chinese Medicine, Changchun, Jilin, China

<sup>b</sup>Jilin Ginseng Academy, Changchun University of Chinese Medicine, Changchun, Jilin, China

## ARTICLE INFO

### Keywords:

Acute pneumonia  
Liquid chromatography-mass spectrometry  
Metabolomics  
Network pharmacology  
Zhuye Shigao decoction

## ABSTRACT

The traditional Chinese medicine (TCM) formulation Zhuye Shigao Decoction (ZSD) has demonstrated therapeutic efficacy in the treatment of acute pneumonia. Nevertheless, the precise mechanisms underlying its pharmacological action remain inadequately elucidated. This study aims to assess the therapeutic efficacy of ZSD in managing acute pneumonia and to elucidate the potential mechanisms driving its effects. A lipopolysaccharide (LPS)-induced murine model of acute pneumonia was established. Histopathological examination and serum biochemical assays were conducted to assess the therapeutic efficacy of ZSD for acute pneumonia. An LC-MS-based metabolomics strategy was employed to explore the impact of ZSD on the serum metabolome. To further elucidate the underlying mechanisms of ZSD's therapeutic effects, a combined metabolomics and network pharmacology strategy was employed. Compared with the model group, ZSD demonstrated the ability to reduce serum levels of Tumor necrosis factor  $\alpha$  (TNF- $\alpha$ ), Interleukin-1 $\beta$  (IL-1 $\beta$ ), and Interleukin-6 (IL-6), while simultaneously enhancing the expression of IgA and IgM. Histological analysis showed that ZSD could significantly improve lung tissue changes caused by LPS exposure. We selected 74 serum metabolites as metabolic biomarkers for acute pneumonia, of which 67 demonstrated significant recovery following treatment with ZSD, thereby highlighting its therapeutic potential in addressing LPS-induced pneumonia. Network pharmacology analysis identified potential targets, including AKT1, IL-6, IL-1 $\beta$ , TNF, Myc proto-oncogene protein (MYC), and Peroxisome proliferator-activated receptor gamma (PPARG). The joint analysis indicated that the potential therapeutic mechanism of ZSD might be associated with sphingolipid metabolism, arachidonic acid metabolism, glycerophospholipid metabolism, PPAR signaling pathway, and Janus kinase-signal transducer and activator of transcription ((JAK-STAT) signaling pathway. This study illustrated the comprehensive regulatory role of ZSD in the treatment of acute pneumonia and, for the first time, elucidated the possible mechanisms of ZSD at both the protein and metabolic levels. Furthermore, it offers a new perspective on the pharmacological effects of Chinese materia medica (CMM) in acute pneumonia treatment, with a particular emphasis on metabolic regulation.

## 1. Introduction

Acute pneumonia is a clinical condition characterized by impaired respiratory immunity and compromised barrier functions, typically triggered by bacterial, viral, or other pathogenic infections. Clinically, it presents with hallmark symptoms like high fever, cough, chest tightness, dyspnea, and loss of appetite [1]. It shows higher mortality rates in immunocompromised children and elderly individuals [2]. Although antibiotics are primarily used in the clinical treatment of acute pneumonia, their widespread use has contributed to the emergence of bacterial resistance, significantly diminishing the efficacy of monotherapy [3]. Therefore, it is of paramount importance to develop drugs with minimal side effects and robust clinical effects in the prevention and treatment of acute pneumonia.

Compared with the symptomatic treatment approach of modern medicine, traditional Chinese medicine (TCM) pays more attention to

the holistic concept, treating pneumonia patients as integrated systems and tailoring therapeutic strategies to specific syndrome types. These strategies include evacuating wind and cold, promoting lung and relieving cough, clearing heat and dissolving phlegm, etc. [4]. A classic prescription Zhuye Shigao decoction (ZSD) comes from the "Shang Han Za Bing Lun" written by Zhang Zhongjing in the Han Dynasty, which includes Folium phyllostachydis henonis, Gypsum fibrosum, Ginseng radix et rhizoma, Ophiopogonis radix, Pinelliae rhizoma, Glycyrrhizae radix et rhizoma, Oryze semen. This formula is traditionally recognized for its ability to clear heat, promote salivation, tonify qi, and regulate the stomach. With a history of over 1000 years, its efficacy on acute pneumonia has also been confirmed in modern clinical practice [5]. Studies have shown that ZSD combined with Yinqiaosan achieved a 91.115 effective rate for severe pneumonia [6]. The combination of ZSD and Maidong decoction showed remarkable efficacy in addressing drug-resistant community-acquired pneumonia, with a reported

### \*Corresponding author:

E-mail address: wang.yang1986@hotmail.com (Y. Wang)

<sup>†</sup>Authors contributed equally to this work and shared co-first authorship.

Received: November, 2024 Accepted: March, 2025 Epub Ahead of Print: 14 May 2025 Published: 21 May 2025

DOI: 10.25259/AJC\_192\_2024

effective rate of 97.44% [7]. Despite these promising outcomes, its mechanism of action is still unclear. Given the complex composition of ZSD, elucidating its mechanism of action requires the integration of advanced modern techniques, such as omics and comprehensive network pharmacology analysis [8].

Metabolomics, an emerging scientific discipline, focuses on the comprehensive analysis of small molecules within biochemical samples. This strategy provides valuable insights into metabolite fluctuations during metabolic processes and uncovers the interaction and regulatory mechanisms among these metabolites [9]. Changes in the metabolome serve as direct indicators of metabolic network activity and provide foundational information regarding the underlying biological state of the system. As a holistic strategy to understand systemic characteristics, metabolomics aligns seamlessly with the TCM principles of “holistic concept” and “therapy with syndrome differentiation”, which provides new ideas for the modernization of TCM [10, 11]. Network pharmacology, on the other hand, creates biological network models, such as drug-target and gene-disease networks, to investigate the active compounds in Chinese materia medica (CMM), predict their potential targets, and explore their associations with various diseases [12]. This approach enables the identification of multi-target and multi-pathway mechanisms inherent to CMM, providing a theoretical foundation for its research, development, and clinical application. Through the network pharmacology approach, various components in ZSD can be summarized and screened to determine the principal active compounds. Moreover, the mechanism of action of ZSD can be elucidated by mapping the intricate network of interactions between the drug and biomolecules.

In this study, the chemical composition of the ZSD extract was characterized using ultra-high-performance liquid chromatography coupled with high-resolution mass spectrometry (UHPLC-HRMS). The lipopolysaccharide (LPS)-induced acute pneumonia mice model was established, and ZSD was administered *via* intragastric gavage. The serum metabolic biomarkers were selected by LC-MS-based untargeted metabolomics analysis. The network pharmacology approach was employed to investigate the potential therapeutic targets of ZSD in mice with LPS-induced acute pneumonia. The joint pathway analysis, integrating altered serum metabolites and active targets, was further applied to reveal the potential mechanistic action of ZSD in the treatment of acute pneumonia. This study demonstrated that ZSD could exert therapeutic effects on acute pneumonia by modulating endogenous metabolite levels through a comprehensive regulation of the component-target-pathway network. This finding provides robust scientific evidence supporting the clinical application of ZSD in the treatment of acute pneumonia.

## 2. Materials and Methods

### 2.1. Chemicals and reagents

HPLC-grade acetonitrile and methanol were purchased from Fisher Scientific Corporation (Waltham, USA). Formic acid was provided by Aladdin Industrial Corporation (Shanghai, China). The purified water was obtained from Watsons (Guangzhou, China). All traditional herbal medicines listed in Table 1 were provided by Hebei Shenwei Pharmaceutical Co., Ltd. (Shijiazhuang, China). The voucher specimens of these CMMs were deposited at the laboratory of Chinese medicine analysis with the labels ZSD2024001-2024007. Lipopolysaccharide (N28IS220883) was purchased from Shanghai Yuanye Biological Co.,

Ltd. (Shanghai, China). Dexamethasone acetate tablets (2306152) were purchased from Suicheng Pharmaceutical Co., Ltd. (Zhengzhou, China). The enzyme-linked immunosorbent assay (ELISA) kits were purchased from Shanghai Youxuan Biotechnology Co., Ltd. (Shanghai, China).

### 2.2. Preparation of ZSD

The preparation process of ZSD was established based on preliminary experimental research conducted in our laboratory. The CMMs, comprising 27.6 g of Zhuye, 27.7 g of Renshen, 34.5 g of Banxia, 106 g of Maidong, 220 g of Shigao, and 27.6 g of Gancao, were precisely weighed and subsequently decocted in 2 L of boiling water for a duration of 30 mins. After being filtered with a 200 mesh gauze, Jingmi (110 g) was added to the filtrate and decocted for 20 mins. Then, it was filtered by gauze, and the filtrate was concentrated at 800 mL to obtain standard decoction. The decoction was freeze-dried and stored.

### 2.3. Characterization of ZSD by UHPLC-MS

The freeze-dried ZSD powder (1 g) was precisely weighed and combined with a methanol/water (1:1) solvent mixture (20 mL). Following ultrasonic extraction for 30 mins, the resultant extract was filtered through a 0.22 µm microporous membrane prior to LC-MS analysis. The Mass spectrometry (MS) and MS/MS spectra of ZSD were acquired using full-scan and fast-data-dependent acquisition (DDA) modes, which were utilized to conduct compound annotation and identification through database searching. The detailed LC-MS methods are shown in Supplementary Materials. The data processing was conducted using MS-DIAL software [13], and the parameters were set as follows: Data collection, MS1 tolerance 0.01 Da and MS2 tolerance 0.025Da; Peak detection, Minimum peak height 1000 amplitude and Mass slice width 0.1 Da; Adduct, [M-H]<sup>-</sup>, [M-H<sub>2</sub>O-H]<sup>-</sup>, [M+FA-H]<sup>-</sup>, [M+H]<sup>+</sup>, [M+Na]<sup>+</sup>. Compound annotation was performed by comparing the acquired MS and MS/MS data against database records. The MSP format databases, including MSMS\_Public\_EXP\_NEG\_VS17 and MSMS\_Public\_EXP\_Pos\_VS17, were obtained from <https://systemsomicslab.github.io/compms/msdial/main.html#MSP> and subsequently imported into the MS-DIAL software for database searching.

### 2.4. Animals and treatment

Fifty Institute of Cancer Research (ICR) male mice, weighing 35±2g, were provided by Changchun Yisi Animal Co., Ltd. (Changchun, China). The feeding temperature is maintained at 20-25°C, with relative humidity ranging from 40% to 55%, and a 12-hr light-dark cycle in a climate-controlled environment. The Animal Ethics Committee of the Changchun University of Chinese Medicine approved the whole animal treatment (approval number: 2024313). Following a one-week acclimation period, 50 mice were randomly allocated into five distinct groups, each comprising 10 mice. These groups were designated as control, model, positive, ZSD low-dose (ZSD-L), and ZSD high-dose (ZSD-H).

The mouse model was established according to the literature document with slight modifications [14]. The anesthetized mice were positioned on a 45-degree inclined platform. The mouth of each mouse was gently opened, and the tongue was carefully extended using tweezers. A pipette was used to administer 50 µL of a 1 g/L LPS solution. The control group received an equivalent volume of normal

Table 1. The information on purchased CMM.

No.	Latin name	English name	Chinese name	Batch No.
1	<i>Phyllostachys nigra</i> (Lodd.) Munro var. <i>henonis</i> (Mitf.) Stapf ex Rendle.	Folium phyllostachydis henonis	Zhuye	BZ230701
2	Gypsum Fibrosum	Gypsum fibrosum	Shigao	1709271
3	<i>Panax ginseng</i> C. A. Mey.	Ginseng radix et rhizoma	Renshen	23072301
4	<i>Ophiopogon japonicus</i> (L.f) Ker-Gawl.	Ophiopogonis radix	Maidong	20190602
5	<i>Pinellia ternata</i> (Thunb.) Breit.	Pinelliae rhizoma	Banxia	XH22082201
6	<i>Glycyrrhiza uralensis</i> Fisch.	Glycyrrhizae radix et rhizoma	Gancao	HIQ23041501
7	<i>Oryza sativa</i> L. subsp. <i>japonica</i> Kato.	Oryze semen	Jingmi	HL24012101

saline, which was slowly instilled into the posterior pharyngeal wall of the mice. Simultaneously, the noses of the mice were pinched for 30 seconds to ensure ingestion, after which the tongue and nose were released, allowing the mice to recover naturally in their cages. Following a two-day modeling period, all groups, with the exception of the control and model groups, received their respective treatments for seven consecutive days: the positive control group was administered dexamethasone (0.6 mg/kg, i.g.), the ZSD-L group received ZSD at a dosage of 5.2 g/kg (i.g.), and the ZSD-H group was given ZSD at a dosage of 10.4 g/kg (i.g.).

The mice were humanely euthanized 12 hrs after final administration, by an intraperitoneal 10% chloral hydrate injection. Blood samples were then collected and divided into two aliquots for subsequent biochemical and metabolomics analyses. The left lobe of the lung was immersed in a 4% formaldehyde solution for histopathological examination.

## 2.5. Histopathological analysis

The lung tissue was fixed overnight in 4% paraformaldehyde, embedded in paraffin, and stained with hematoxylin and eosin (HE). The pathological state of lung tissue was observed under a microscope.

## 2.6. Serum inflammatory cytokines and immunoglobulin analysis

The blood samples were left to clot at ambient temperature for 30 mins, followed by centrifugation at 3000 g for 15 mins at 4°C. The resultant supernatant serum was collected for subsequent biochemical analyses. The concentrations of inflammatory cytokines, specifically tumor necrosis factor  $\alpha$  (TNF- $\alpha$ ), interleukin-1 $\beta$  (IL-1 $\beta$ ), and interleukin-6 (IL-6), along with immunoglobulins A (IgA) and M (IgM), were quantified utilizing the appropriate enzyme-linked immunosorbent assay (ELISA) kits.

## 2.7. Serum metabolic profile

### 2.7.1. Serum sample preparation and data acquisition

The serum sample was prepared using our previous protocols [15]. Metabolomics focuses on the small molecules in a given biological sample; thus, the organic solvent is always used to remove protein and extract metabolite. In this study, a serum sample of 100  $\mu$ L was combined with 300  $\mu$ L of methanol to facilitate protein precipitation. The resulting mixture underwent centrifugation at 15000 g for 15 mins at 4°C. Subsequently, the supernatant was evaporated under a nitrogen stream and reconstituted in 100  $\mu$ L of ultrapure water. Following a second centrifugation at 15000 g for 15 mins at 4°C, an aliquot of 5  $\mu$ L from the supernatant was injected into the LC-MS system to acquire the metabolic profile of the serum samples.

LC-MS has high resolution, sensitivity, and throughput merits, so it is considered a major platform for untargeted metabolomics analysis. In this study, an LC-MS-based untargeted metabolomics strategy was applied to analyze the prepared serum samples and to screen the metabolites associated with animal modeling and ZSD intervention. Since a column with sub 2  $\mu$ m particle size packing could offer excellent chromatographic separation resolution, fast analysis speed, and high detection sensitivity, we chose a C18 column with 1.7  $\mu$ m to analyze serum samples with the complex matrix. MS detection was conducted on a Q-TOF MS instrument, during which the full scan was applied to obtain the MS information of metabolites acquired for data preprocessing, and the fast-DDA was conducted to acquire the MS/MS spectra of features for compound annotation. Before commencing sample analysis, the precision of the MS instrument was calibrated with standard reagents. The real-time calibration was conducted concurrently with sample analysis to ensure the MS accuracy. For the detailed LC-MS setting, please refer to the [Supplementary Material](#).

### 2.7.2. Data analysis

Progenesis QI software (Nonlinear Dynamics, Newcastle, UK) was employed for preprocessing raw data and organizing all chromatograms into a comprehensive dataset that included sample groups, peak retention times (RT), mass-to-charge ratios (m/z), and peak intensities

for subsequent statistical analyses. Utilizing SIMCA 14.1 software, a partial least squares discriminant analysis (PLS-DA) model was developed based on this dataset. The variable importance in projection (VIP) value of each feature was calculated to assess the significance of variables, with features exhibiting VIP values greater than 1 deemed most critical for sample classification. Metabolic biomarkers associated with LPS-induced acute pneumonia were identified by combining the VIP value with a fold change (FC) >2 and a t-test P value < 0.05. Metabolite annotation was conducted by querying the Human Metabolome Database (HMDB) [16] using the precise m/z and MS/MS data of the extracted features. Subsequently, the HMDB identifiers of the annotated metabolites were input into the MetaboAnalyst 6.0 web tool [17] for metabolic pathway analysis.

## 2.8. Network pharmacology analysis

### 2.8.1. Selection of CMM compounds and related targets

The Traditional Chinese Medicine Systems Pharmacology (TCMSP) database [18] was employed to investigate the chemical constituents of CMM, utilizing the keywords "Ginseng," "Glycyrrhiza uralensis Fisch," and "Pinellia ternata." Compounds exhibiting an oral bioavailability (OB) of  $\geq 30\%$  and a drug-likeness (DL) index of  $\geq 0.18$  were regarded as active ingredients. Given that TCMSP does not encompass all CMMs within ZSD, the HERB Database [19] was utilized to identify the active compounds present in bamboo leaves and *Ophiopogon japonicus*. The targets that these active ingredients can regulate were identified and validated using the UniProt Database [20], excluding non-human targets. Consequently, the drug targets of ZSD were ascertained.

### 2.8.2. Disease target selection and drug-active ingredient-target network construction

The disease target was identified using the GeneCards database [21] with "Acute pneumonia" as the search term. The active ingredients and associated targets of ZSD, along with pneumonia-related targets, were systematically organized in an Excel spreadsheet and subsequently imported into Cytoscape 3.9.1 software [22] to construct a Chinese Materia Medica-active ingredient-target (CMM-AI-T) network. A Venn diagram drawing web tool (<https://bioinformatics.psb.ugent.be/webtools/Venn/>) was employed to determine the intersection between ZSD targets and disease targets, thereby identifying potential therapeutic targets of ZSD for the treatment of acute pneumonia. The overlapping targets were then imported into the Search Tool for the Retrieval of Interacting Genes (STRING) database [23] to develop a protein-protein interaction (PPI) network with a confidence threshold greater than 0.9. TSV format files of the PPI networks were downloaded and imported into Cytoscape 3.9.1 software to facilitate network visualization, conduct topological analysis, and identify core targets.

## 3. Results and Discussion

### 3.1. Characterisation of the chemical composition of ZSD

The chemical composition of ZSD was characterized using UPLC-Q-TOF MS, employing both positive and negative ion modes to ensure a comprehensive analysis of the ZSD extract. The base peak chromatograms (BPC) of ZSD, acquired under different ionization conditions, have been illustrated in [Figure 1\(a\)](#) and [1\(b\)](#). Following database interrogation, 107 compounds were identified and annotated in ZSD, predominantly terpenoids, flavonoids, and saponins, as detailed in [Table 2](#). To exemplify the annotation results, we used three representative compounds as examples.

The mass spectrum of a saponin (#68) at RT 6.79 min, m/z 991.5468 has been shown in [Figure 1\(c\)](#), in which the precursor of m/z 991.5468 coeluted with ions at m/z 233.0861 and m/z 845.5468. The MS/MS spectrum of the ion with m/z 991.5468 has been presented in [Figure 1\(d\)](#). The base peak at m/z 945.5604 exhibits a  $\Delta m/z$  of 46 Da relative to the precursor, suggesting that the precursor ion is [M+HCOO]<sup>-</sup>, while the ion at m/z 945.5604 represents the deprotonated molecule. Additionally, the fragment ion at m/z 637.4652 results from the loss of a saccharide moiety at the C6 position. The ion at m/z 475.4009 was

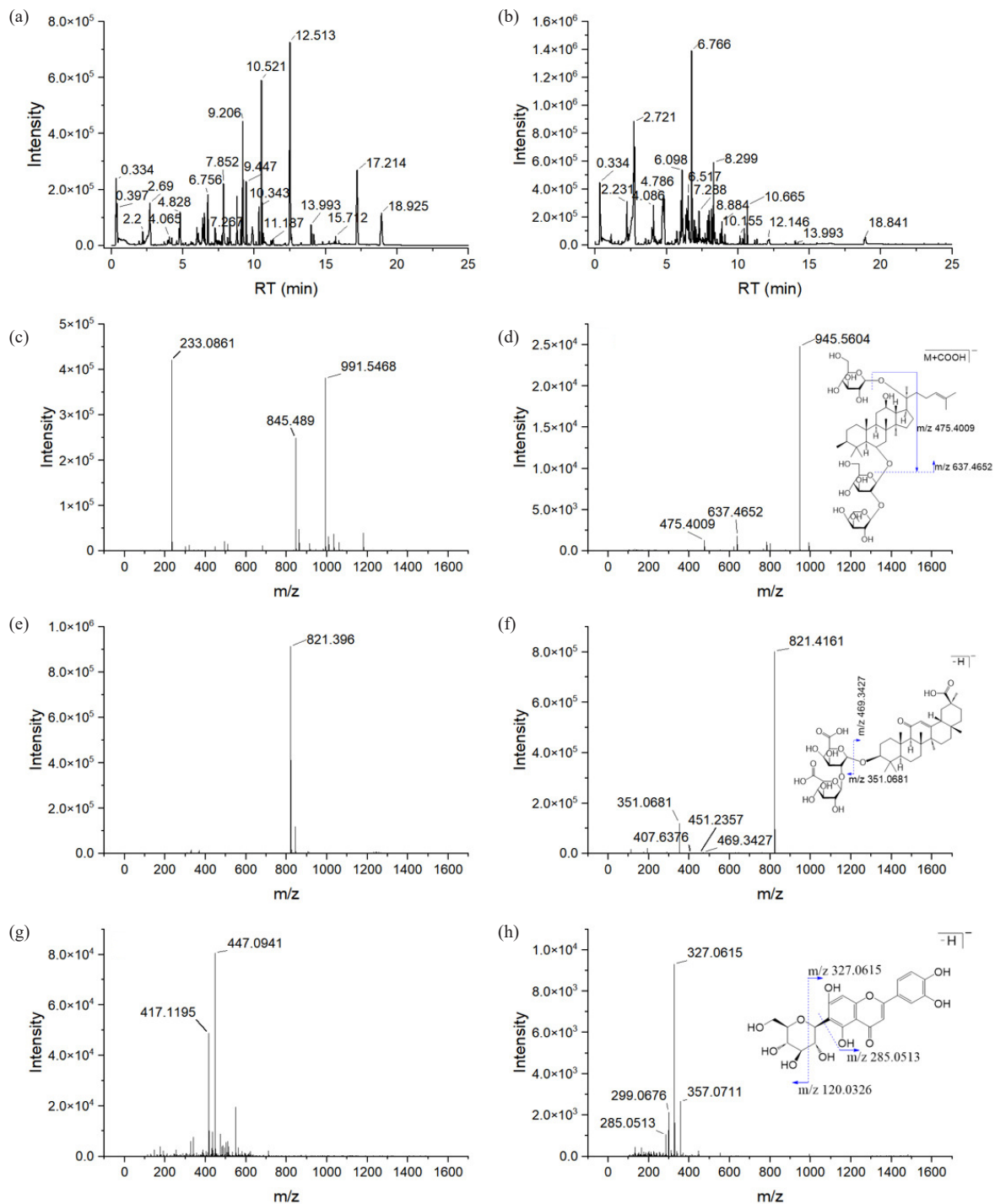


**Figure 1.** Characterization of the chemical composition of ZSD. The BPCs of ZSD were obtained from both (a) positive and (b) negative ion modes. MS and MS spectra are presented for (c-d) ginsenoside Re, (e-f) glycyrrhizic acid, and (g-h) isorhizobin.

identified as  $[M-H-2Glc-Rha]^-$ . Based on the information provided, the compound #68 was assigned to ginsenoside Re.

The MS and MS/MS spectra of compound #66 at RT 6.72 min,  $m/z$  821.3960 have been shown in Figure 1(e) and 1(f). The deprotonated molecule with an  $m/z$  value of 821.3960 is identified as the base peak in the MS spectrum. Fragment ions with  $m/z$  values of 469.3427 and 351.0681 are attributed to  $[M-H-gluA-gluA]^-$  and represent two molecules of glucuronic acid, respectively. The ion at  $m/z$  451.2357 is generated by the loss of an  $H_2O$  molecule from  $[M-H-gluA-gluA]^-$ , while the ion at  $m/z$  407.6376 corresponds to  $[M-H-gluA-gluA-H_2O-CO_2]^-$ . Collectively, this compound was annotated as glycyrrhizic acid.

As illustrated in Figure 1(g), the MS spectrum of compound #8 reveals a base peak at  $m/z$  447.0941, which corresponds to the  $[M-H]^-$  ion. The MS/MS spectrum, depicted in Figure 1(h), displays ions at  $m/z$  285.0513 and  $m/z$  327.0615, corresponding to the  $[M-H-glc]^-$  and  $[M-120.0326]^-$  ions, respectively. Therefore, this compound was assigned to isoorientin, which is a flavonoid.

### 3.2. Effect of ZSD on acute pneumonia

Histological examination using HE staining was conducted on lung tissue sections to evaluate morphological alterations and determine

**Table 2.** The chemical composition of ZSD detected by UHPLC-MS.

No.	Compound name	RT (min)	Detected m/z	Theoretical m/z	Adducts	Molecular Formula	Mass error (ppm)	Origin
1	Methocarbamol	0.35	242.1045	242.1023	[M <sup>+</sup> H] <sup>+</sup>	C <sub>11</sub> H <sub>15</sub> NO <sub>5</sub>	9.09	-
2	Xanthotoxin	0.38	215.0329	215.0350	[MH] <sup>-</sup>	C <sub>22</sub> H <sub>8</sub> O <sub>4</sub>	-9.67	a
3	Fumaric acid	0.38	115.0044	115.0037	[MH] <sup>-</sup>	C <sub>4</sub> H <sub>2</sub> O <sub>4</sub>	6.26	b
4	Scutellarioside II	0.38	507.1551	507.1508	[MH] <sup>-</sup>	C <sub>24</sub> H <sub>28</sub> O <sub>12</sub>	8.48	a, e
5	Adenosine	0.42	268.1058	268.1040	[M <sup>+</sup> H] <sup>+</sup>	C <sub>10</sub> H <sub>13</sub> N <sub>5</sub> O <sub>4</sub>	6.60	d
6	debromohymenialdisine	0.42	246.0996	246.0986	[M <sup>+</sup> H] <sup>+</sup>	C <sub>11</sub> H <sub>11</sub> N <sub>5</sub> O <sub>2</sub>	4.27	c
7	Citric acid	0.45	191.0197	191.0197	[MH] <sup>-</sup>	C <sub>6</sub> H <sub>8</sub> O <sub>7</sub>	-0.16	b
8	Isoorientin	0.85	447.0915	447.0933	[MH] <sup>-</sup>	C <sub>21</sub> H <sub>20</sub> O <sub>11</sub>	-4.00	a
9	Isobavachin	1.05	323.1231	323.1289	[MH] <sup>-</sup>	C <sub>20</sub> H <sub>20</sub> O <sub>4</sub>	-17.89	a
10	3-(3-Hydroxyphenyl)propionic acid	1.11	165.0565	165.0557	[MH] <sup>-</sup>	C <sub>9</sub> H <sub>10</sub> O <sub>3</sub>	4.73	a
11	Epicatechin-3-o-gallate	1.11	441.0791	441.0827	[MH] <sup>-</sup>	C <sub>22</sub> H <sub>18</sub> O <sub>10</sub>	-8.21	b
12	verruculotoxin	1.12	262.1928	262.1914	[M <sup>+</sup> NH <sub>4</sub> ] <sup>+</sup>	C <sub>15</sub> H <sub>20</sub> N <sub>2</sub> O	5.38	c, e
13	Kynurenic acid	1.12	190.0507	190.0499	[M <sup>+</sup> H] <sup>+</sup>	C <sub>10</sub> H <sub>7</sub> NO <sub>3</sub>	4.37	a
14	Shikimic Acid	1.32	173.0457	173.0456	[MH] <sup>-</sup>	C <sub>7</sub> H <sub>10</sub> O <sub>5</sub>	0.87	-
15	Chlorogenic acid	1.32	353.0878	353.0878	[MH] <sup>-</sup>	C <sub>16</sub> H <sub>18</sub> O <sub>9</sub>	-0.03	a
16	(3-Formyl-2,4-dihydroxy-6-methylbenzoic acid (2-carboxy-3,5-dihydroxy-4-methylphenyl)methyl ester) Alectorialic acid	1.32	375.0688	375.0722	[MH] <sup>-</sup>	C <sub>18</sub> H <sub>16</sub> O <sub>9</sub>	-8.96	-
17	eupomatenoid 5	1.35	293.116	293.1183	[MH] <sup>-</sup>	C <sub>13</sub> H <sub>18</sub> O <sub>3</sub>	-7.91	b
18	Citrinin	1.39	249.0791	249.0769	[MH] <sup>-</sup>	C <sub>13</sub> H <sub>14</sub> O <sub>5</sub>	9.03	c, e
19	Liquiritin	1.56	417.1185	417.1191	[MH] <sup>-</sup>	C <sub>24</sub> H <sub>22</sub> O <sub>9</sub>	-1.46	e
20	Naringin	1.57	603.1666	603.1684	[M <sup>+</sup> Na] <sup>+</sup>	C <sub>27</sub> H <sub>32</sub> O <sub>14</sub>	-3.03	b, e
21	Rutin	1.66	609.1465	609.1461	[MH] <sup>-</sup>	C <sub>27</sub> H <sub>30</sub> O <sub>16</sub>	0.64	a
22	5-Demethylnobiletin	1.84	387.1071	387.1085	[MH] <sup>-</sup>	C <sub>20</sub> H <sub>20</sub> O <sub>8</sub>	-3.72	c, d
23	Methyl chlorogenate	2.02	367.1045	367.1035	[MH] <sup>-</sup>	C <sub>17</sub> H <sub>20</sub> O <sub>9</sub>	2.83	a
24	Luteolin 7-O-glucoside	2.17	447.0943	447.0933	[MH] <sup>-</sup>	C <sub>21</sub> H <sub>20</sub> O <sub>11</sub>	2.26	a
25	Orientin	2.17	447.0901	447.0922	[MH] <sup>-</sup>	C <sub>21</sub> H <sub>20</sub> O <sub>11</sub>	-4.67	a
26	Apiin	2.21	563.143	563.1406	[MH] <sup>-</sup>	C <sub>26</sub> H <sub>28</sub> O <sub>14</sub>	4.21	e
27	Phenprobamate	2.25	180.1009	180.1019	[M <sup>+</sup> H] <sup>+</sup>	C <sub>10</sub> H <sub>13</sub> NO <sub>2</sub>	-5.61	-
28	Tetrahydropapaveroline	2.49	288.1235	288.1230	[M <sup>+</sup> H] <sup>+</sup>	C <sub>16</sub> H <sub>17</sub> NO <sub>4</sub>	1.63	-
29	bungeiside C	2.51	453.1364	453.1367	[M <sup>+</sup> H] <sup>+</sup>	C <sub>19</sub> H <sub>26</sub> O <sub>11</sub>	-0.73	-
30	vitexin	2.64	433.1144	433.1129	[M <sup>+</sup> H] <sup>+</sup>	C <sub>21</sub> H <sub>20</sub> O <sub>10</sub>	3.42	a
31	Convallatoxin	2.71	549.2704	549.2705	[MH] <sup>-</sup>	C <sub>29</sub> H <sub>42</sub> O <sub>10</sub>	-0.22	a, b, c, e
32	N-lauroylsarcosine	2.81	272.2244	272.2220	[M <sup>+</sup> H] <sup>+</sup>	C <sub>15</sub> H <sub>29</sub> NO <sub>3</sub>	8.74	d
33	Agnuside	3.00	467.1538	467.1548	[M <sup>+</sup> H] <sup>+</sup>	C <sub>22</sub> H <sub>26</sub> O <sub>11</sub>	-2.12	a
34	Dihydrohesperetin-7-O-neohesperidoside	3.06	611.1951	611.1981	[MH] <sup>-</sup>	C <sub>28</sub> H <sub>36</sub> O <sub>15</sub>	-4.97	a
35	(2-hydroxy-4-methoxy-6-propylbenzoic acid) Divaricatinic acid	3.11	209.0824	209.0819	[MH] <sup>-</sup>	C <sub>11</sub> H <sub>14</sub> O <sub>4</sub>	2.25	-
36	Baicalein	3.22	269.0464	269.0456	[MH] <sup>-</sup>	C <sub>15</sub> H <sub>10</sub> O <sub>5</sub>	3.16	d
37	Diosmetin	3.32	299.0569	299.0561	[MH] <sup>-</sup>	C <sub>16</sub> H <sub>12</sub> O <sub>6</sub>	2.64	b, e
38	Homoeriodictyol	3.38	301.0727	301.0718	[MH] <sup>-</sup>	C <sub>16</sub> H <sub>14</sub> O <sub>6</sub>	3.12	a, c, e
39	Sissotrin	3.67	491.1185	491.1195	[M <sup>+</sup> HCOO] <sup>-</sup>	C <sub>22</sub> H <sub>22</sub> O <sub>10</sub>	-2.04	e
40	Jaceosidin	3.68	331.0826	331.0812	[M <sup>+</sup> H] <sup>+</sup>	C <sub>17</sub> H <sub>14</sub> O <sub>7</sub>	4.14	c
41	Albiflorin	3.70	481.1672	481.1704	[M <sup>+</sup> H] <sup>+</sup>	C <sub>23</sub> H <sub>28</sub> O <sub>11</sub>	-6.73	-
42	Liquiritin apioside	3.91	573.1534	573.1579	[M <sup>+</sup> Na] <sup>+</sup>	C <sub>26</sub> H <sub>30</sub> O <sub>13</sub>	-7.78	e
43	Paprazine	3.94	284.1295	284.1281	[M <sup>+</sup> H] <sup>+</sup>	C <sub>17</sub> H <sub>17</sub> NO <sub>3</sub>	4.86	c
44	Isoliquiritin	4.03	419.1341	419.1337	[M <sup>+</sup> H] <sup>+</sup>	C <sub>21</sub> H <sub>22</sub> O <sub>9</sub>	1.05	e
45	Liquiritigenin	4.03	255.0678	255.0663	[MH] <sup>-</sup>	C <sub>15</sub> H <sub>12</sub> O <sub>4</sub>	5.96	e
46	Digitonin	4.09	1273.571	1273.5706	[M <sup>+</sup> HCOO] <sup>-</sup>	C <sub>56</sub> H <sub>92</sub> O <sub>29</sub>	0.29	c
47	licochalcone B	4.16	287.0914	287.0914	[M <sup>+</sup> H] <sup>+</sup>	C <sub>16</sub> H <sub>14</sub> O <sub>5</sub>	0.00	e
48	7-O-Methylchrysin	4.20	269.0826	269.0808	[M <sup>+</sup> H] <sup>+</sup>	C <sub>16</sub> H <sub>12</sub> O <sub>4</sub>	6.54	-
49	Salvianolic acid C	4.20	515.0898	515.0949	[M <sup>+</sup> Na] <sup>+</sup>	C <sub>26</sub> H <sub>20</sub> O <sub>10</sub>	-9.84	b, e
50	Homoharringtonine	4.37	568.249	568.2517	[M <sup>+</sup> Na] <sup>+</sup>	C <sub>20</sub> H <sub>39</sub> NO <sub>9</sub>	-4.75	c
51	Ginsenoside Rf	4.72	823.4821	823.4814	[M <sup>+</sup> Na] <sup>+</sup>	C <sub>42</sub> H <sub>72</sub> O <sub>14</sub>	0.81	b
52	Rhodojaponin III	4.98	391.2085	391.2091	[M <sup>+</sup> Na] <sup>+</sup>	C <sub>20</sub> H <sub>32</sub> O <sub>6</sub>	-1.56	b, e
53	Tricin	5.56	331.0824	331.0812	[M <sup>+</sup> H] <sup>+</sup>	C <sub>17</sub> H <sub>14</sub> O <sub>7</sub>	3.53	a

(Contd...)

(Contd...)

No.	Compound name	RT (min)	Detected m/z	Theoretical m/z	Adducts	Molecular Formula	Mass error (ppm)	Origin
54	Arjungenin	5.70	527.3358	527.3343	[M <sup>+</sup> Na] <sup>+</sup>	C <sub>30</sub> H <sub>48</sub> O <sub>6</sub>	2.83	d
55	Undecanedioic acid	5.71	215.1296	215.1289	[MH] <sup>-</sup>	C <sub>11</sub> H <sub>20</sub> O <sub>4</sub>	3.35	a, b, c, d, e
56	Hispidulin	5.82	299.0563	299.0561	[MH] <sup>-</sup>	C <sub>16</sub> H <sub>12</sub> O <sub>6</sub>	0.64	e
57	Caperatic acid	5.84	425.2512	425.2510	[M <sup>+</sup> Na] <sup>+</sup>	C <sub>21</sub> H <sub>38</sub> O <sub>7</sub>	0.54	e
58	Nandrolone	6.03	275.2014	275.2006	[M <sup>+</sup> H] <sup>+</sup>	C <sub>18</sub> H <sub>26</sub> O <sub>2</sub>	3.05	a, b, c
59	Ginsenoside Rg1	6.10	845.4884	845.4904	[MH] <sup>-</sup>	C <sub>42</sub> H <sub>72</sub> O <sub>14</sub>	-2.38	b
60	Pazopanib	6.14	438.1722	438.1707	[M <sup>+</sup> H] <sup>+</sup>	C <sub>21</sub> H <sub>23</sub> N <sub>7</sub> O <sub>2</sub> S	3.49	-
61	Formononetin	6.24	267.0673	267.0663	[MH] <sup>-</sup>	C <sub>16</sub> H <sub>12</sub> O <sub>4</sub>	3.82	a, b, d, e
62	Ginsenoside F3	6.24	815.4769	815.4799	[M <sup>-</sup> HCOO] <sup>-</sup>	C <sub>41</sub> H <sub>70</sub> O <sub>13</sub>	-3.62	b
63	Ginsenoside Rb1	6.38	1153.598	1153.6011	[M <sup>-</sup> HCOO] <sup>-</sup>	C <sub>54</sub> H <sub>92</sub> O <sub>23</sub>	-2.72	b
64	Ginsenoside Rh1	6.45	683.4362	683.4376	[M <sup>-</sup> HCOO] <sup>-</sup>	C <sub>36</sub> H <sub>62</sub> O <sub>9</sub>	-2.03	b
65	Licoricesaponin G2	6.52	837.3901	837.3914	[MH] <sup>-</sup>	C <sub>42</sub> H <sub>62</sub> O <sub>17</sub>	-1.58	e
66	Glycyrrhizic acid	6.72	821.396	821.3965	[MH] <sup>-</sup>	C42H62O16	-0.62	e
67	Licoricesaponin H2	6.76	823.4113	823.4111	[M <sup>+</sup> H] <sup>+</sup>	C42H62O16	0.29	e
68	Ginsenoside Re	6.79	991.5467	991.5483	[M <sup>-</sup> HCOO] <sup>-</sup>	C <sub>48</sub> H <sub>82</sub> O <sub>18</sub>	-1.63	b
69	Octyl-methoxycinnamate	6.89	291.1971	291.1955	[M <sup>+</sup> H <sub>2</sub> O] <sup>+</sup>	C <sub>18</sub> H <sub>26</sub> O <sub>3</sub>	5.60	a, d, e
70	Fenpropimorph	6.93	304.2654	304.2635	[M <sup>+</sup> H] <sup>+</sup>	C <sub>20</sub> H <sub>33</sub> NO	6.28	a, b, c, d, e
71	Ginsenoside Ro	7.09	957.5066	957.5054	[M <sup>+</sup> H] <sup>+</sup>	C <sub>48</sub> H <sub>76</sub> O <sub>19</sub>	1.30	b
72	Lauryldiethanolamine	7.23	274.2754	274.2741	[M <sup>+</sup> H] <sup>+</sup>	C <sub>16</sub> H <sub>35</sub> NO <sub>2</sub>	4.89	a, b, c, d, e
73	Curcumin	7.28	367.1195	367.1187	[MH] <sup>-</sup>	C <sub>21</sub> H <sub>20</sub> O <sub>6</sub>	2.15	a, b, c, d, e
74	Triacetyl resveratrol	7.42	353.1041	353.1031	[MH] <sup>-</sup>	C <sub>20</sub> H <sub>18</sub> O <sub>6</sub>	2.95	a, b, c, d, e
75	N-Oleylethanolamine	7.45	326.3077	326.3054	[M <sup>+</sup> H] <sup>+</sup>	C <sub>20</sub> H <sub>39</sub> NO <sub>2</sub>	7.17	d
76	Alpha-guaiacolic acid	7.55	339.1244	339.1238	[MH] <sup>-</sup>	C <sub>20</sub> H <sub>20</sub> O <sub>5</sub>	1.77	b, d, e
77	Wulignan A1	7.62	365.1377	365.1359	[M <sup>+</sup> H] <sup>+</sup>	C <sub>20</sub> H <sub>22</sub> O <sub>5</sub>	4.82	a, c
78	Demethoxycurcumin	7.68	337.1083	337.1082	[MH] <sup>-</sup>	C <sub>20</sub> H <sub>18</sub> O <sub>5</sub>	0.44	b, e
79	5-O-methylvisammioside	7.80	453.171	453.1755	[M <sup>+</sup> H] <sup>+</sup>	C <sub>22</sub> H <sub>28</sub> O <sub>10</sub>	-9.97	b, c
80	Octadecanedioic acid	7.83	313.2389	313.2384	[MH] <sup>-</sup>	C <sub>18</sub> H <sub>34</sub> O <sub>4</sub>	1.50	b, c, d, e
81	Ginsenoside Rg2	7.92	829.4956	829.4955	[M <sup>-</sup> HCOO] <sup>-</sup>	C <sub>42</sub> H <sub>72</sub> O <sub>13</sub>	0.12	b
82	Methylpogononone B	8.29	329.1403	329.1384	[M <sup>+</sup> H] <sup>+</sup>	C <sub>19</sub> H <sub>20</sub> O <sub>5</sub>	5.92	c
83	γ-Linolenic acid	8.46	277.2197	277.2173	[MH] <sup>-</sup>	C <sub>18</sub> H <sub>30</sub> O <sub>2</sub>	8.66	d, e
84	Grayanotoxin I	8.49	413.2535	413.2534	[M <sup>+</sup> H] <sup>+</sup>	C <sub>22</sub> H <sub>36</sub> O <sub>7</sub>	0.29	b, c, d, e
85	Prosapogenin A	8.52	745.409	745.4134	[M <sup>+</sup> Na] <sup>+</sup>	C <sub>39</sub> H <sub>62</sub> O <sub>12</sub>	-5.84	b
86	Ginsenoside Rg6	8.77	811.4864	811.4849	[M <sup>-</sup> HCOO] <sup>-</sup>	C <sub>42</sub> H <sub>70</sub> O <sub>12</sub>	1.81	b
87	Kitasamycin	8.87	786.4658	786.4634	[M <sup>+</sup> H] <sup>+</sup>	C <sub>40</sub> H <sub>67</sub> NO <sub>14</sub>	3.01	-
88	Geranylgeranylhydroquinone	9.19	383.2953	383.2945	[M <sup>+</sup> H] <sup>+</sup>	C <sub>26</sub> H <sub>38</sub> O <sub>2</sub>	2.19	-
89	Histamine-trifluoromethyltoluide	9.19	383.2057	383.2053	[M <sup>+</sup> H] <sup>+</sup>	C <sub>19</sub> H <sub>25</sub> F <sub>3</sub> N <sub>4</sub> O	0.99	a, b, c, d, e
90	Ruscogenin	9.27	431.3189	431.3156	[M <sup>+</sup> H] <sup>+</sup>	C <sub>27</sub> H <sub>42</sub> O <sub>4</sub>	7.67	c
91	Vasicinone	9.60	203.0828	203.0815	[M <sup>+</sup> H] <sup>+</sup>	C <sub>11</sub> H <sub>10</sub> N <sub>2</sub> O <sub>2</sub>	6.40	e
92	5-O-methyllicoricidin	9.60	439.2491	439.2479	[M <sup>+</sup> H] <sup>+</sup>	C <sub>27</sub> H <sub>34</sub> O <sub>5</sub>	2.73	e
93	Dodecylbenzenesulfonic acid	9.64	325.184	325.1843	[MH] <sup>-</sup>	C <sub>18</sub> H <sub>30</sub> O <sub>3</sub> S	-0.89	a, b, c, d, e
94	Protolichesterinic acid	11.18	323.2215	323.2228	[MH] <sup>-</sup>	C <sub>19</sub> H <sub>32</sub> O <sub>4</sub>	-3.96	a, b, c, d, e
95	Dehydroeburicoic acid monoacetate	11.32	533.3598	533.3601	[M <sup>+</sup> Na] <sup>+</sup>	C <sub>33</sub> H <sub>50</sub> O <sub>4</sub>	-0.62	a, b, c, d
96	Trans-Vaccenic acid	11.32	281.2495	281.2486	[MH] <sup>-</sup>	C <sub>18</sub> H <sub>34</sub> O <sub>2</sub>	3.20	a, b
97	Hederagenin	11.47	471.3484	471.3480	[MH] <sup>-</sup>	C <sub>30</sub> H <sub>48</sub> O <sub>4</sub>	0.89	e
98	Bullatine B	11.70	460.2629	460.2670	[M <sup>+</sup> Na] <sup>+</sup>	C <sub>26</sub> H39NO6	-8.82	a, b, c, d, e
99	Campesterol	11.98	423.3557	423.3597	[M <sup>+</sup> Na] <sup>+</sup>	C <sub>28</sub> H <sub>48</sub> O	-9.54	b
100	Panasenoside	12.13	633.1463	633.1426	[M <sup>+</sup> Na] <sup>+</sup>	C <sub>27</sub> H <sub>30</sub> O <sub>16</sub>	5.83	b
101	Ochrolifuanine A	12.46	439.29	439.2856	[M <sup>+</sup> H] <sup>+</sup>	C <sub>29</sub> H <sub>34</sub> N <sub>4</sub>	9.97	b, c, d, e
102	Lunarine	12.46	455.2687	455.2653	[M <sup>+</sup> NH <sub>4</sub> ] <sup>+</sup>	C <sub>25</sub> H <sub>31</sub> N <sub>3</sub> O <sub>4</sub>	7.51	a, b, c, d, e
103	Cycloprodigiosin	12.46	322.189	322.1914	[M <sup>+</sup> H] <sup>+</sup>	C <sub>20</sub> H <sub>23</sub> N <sub>3</sub> O	-7.42	-
104	Valinomycin	13.24	1111.629	1111.6384	[2M <sup>+</sup> Na] <sup>+</sup>	C <sub>54</sub> H <sub>90</sub> N <sub>6</sub> O <sub>18</sub>	-8.49	-
105	Ginsenoside compound K	13.31	621.4366	621.4372	[MH] <sup>-</sup>	C <sub>36</sub> H <sub>62</sub> O <sub>8</sub>	-0.95	b
106	Dehydrotumulosic acid	14.51	485.3601	485.3625	[M <sup>+</sup> H] <sup>+</sup>	C <sub>31</sub> H <sub>48</sub> O <sub>4</sub>	-5.03	-
107	Nonacosane	15.16	409.475	409.4768	[M <sup>+</sup> H] <sup>+</sup>	C <sub>29</sub> H <sub>60</sub>	-4.35	b

a, Folium phyllostachydis henonis; b, Ginseng radix et rhizoma; c, Ophiopogonis radix; d, Pinelliae rhizoma; e, Glycyrrhizae radix et rhizoma

the therapeutic effects of ZSD. As illustrated in Figure 2, the model group exhibited significant tissue edema, proliferation of inflammatory infiltrates in alveolar epithelial cells, and dilation of the alveolar wall capillaries compared with the control group (Figure 2b). Notably, administration of the drug led to a reduction in symptoms such as tissue edema and inflammatory infiltration (Figure 2c-e). These findings suggest that ZSD confers a protective effect against LPS-induced acute pneumonia.

The anti-inflammatory properties of ZSD were assessed by measuring the serum levels of the inflammatory cytokines, IgA, and IgM, with results depicted in Figure 3. Relative to the control group, the model group exhibited increased TNF- $\alpha$ , IL-1 $\beta$ , and IL-6 concentration alongside reduced IgA and IgM levels. Following treatment with ZSD, the concentrations of these inflammatory mediators and immune proteins showed a trend towards normalization, aligning more closely with those of the control group.

### 3.3. Validation of LC-MS method for serum metabolomics analysis

Method validation is critical for metabolomics analysis, which ensures that the differences we obtain in our experiments are due to the sample rather than systematic drift or error. The QC samples were

pre-injected three times to ensure the system was well-balanced. During objective sample analysis, one QC sample was injected after every six samples, and data were used to validate the established method. After data preprocessing, two datasets were generated from QC injections using the data obtained from different ionization modes. We calculated the relative standard deviation (RSD) of each ion in these two datasets, which showed that more than 80% of features had RSDs of less than 30%, suggesting the excellent reproducibility and stability of the constructed sample analysis method.

### 3.4. Metabolic difference discovery

LPS administration can provoke pulmonary inflammation in murine models, subsequently altering systemic metabolic pathways. Consequently, serum samples were obtained, and their metabolomic profiles were assessed employing a validated LC-MS technique. The chromatographic peaks of the control, model, and ZSD-H groups exhibit clarity and distinct separation, with notable differences in RT and peak intensities discernible across the chromatograms (Figure 4). Then, a multivariate statistical analysis of serum metabolite data was conducted to archive more precise and intuitive assessments of serum metabolic data. The PLS-DA models were developed utilizing datasets

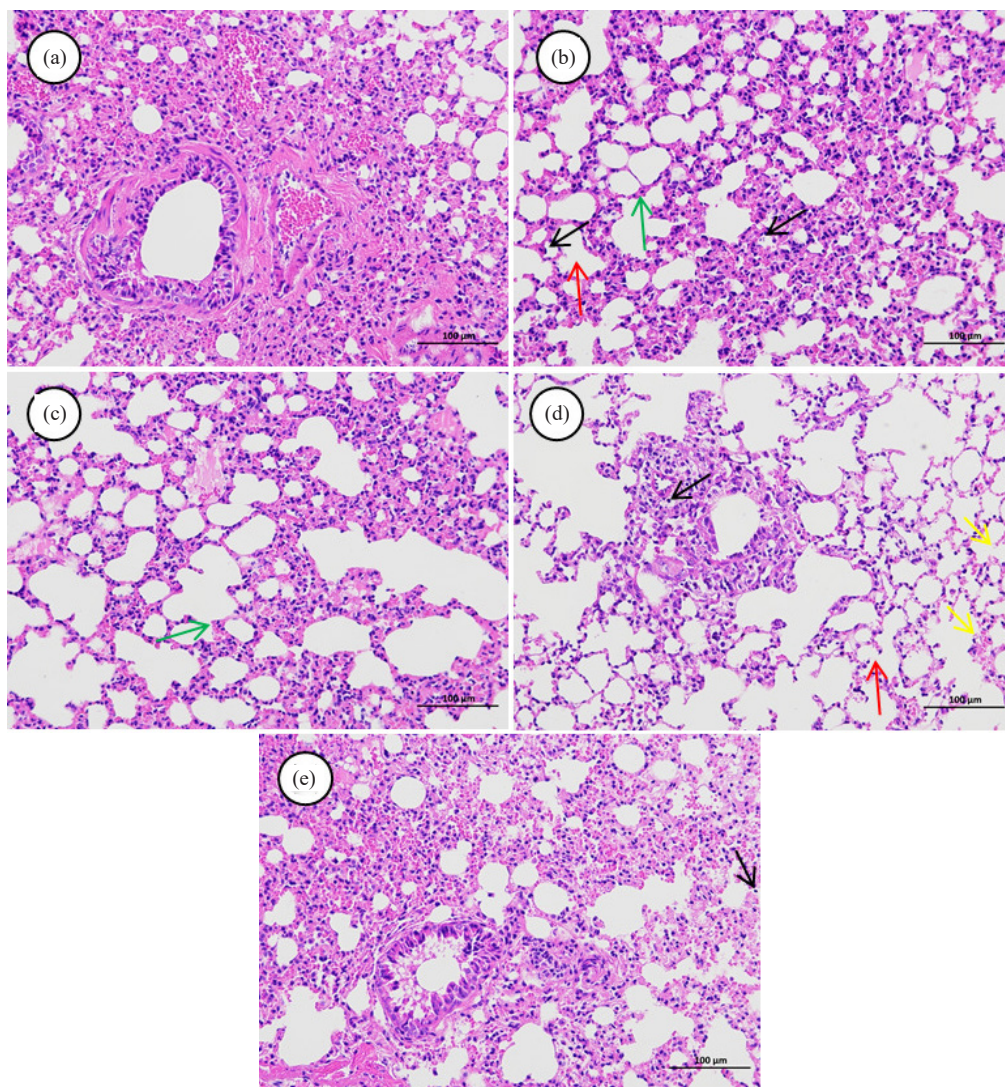


**Figure 2.** Hematoxylin and eosin (HE) stained histopathological sections of lung tissue from the (a) control, (b) model, (c) positive, (d) ZSD-L, and (e) ZSD-H groups. The colored arrows illustrate various histopathological alterations in the lungs under different experimental conditions. (magnification, 200 $\times$ ). (The red arrows denote the partial loss of alveolar septa and the coalescence of alveoli into alveolar sacs. Black arrows indicate widespread infiltration of inflammatory cells within the tissue. Green arrows signify hyperplasia of alveolar epithelial cells and thickening of the alveolar septa. Yellow arrows highlight pronounced capillary dilation in the alveolar wall sections.)

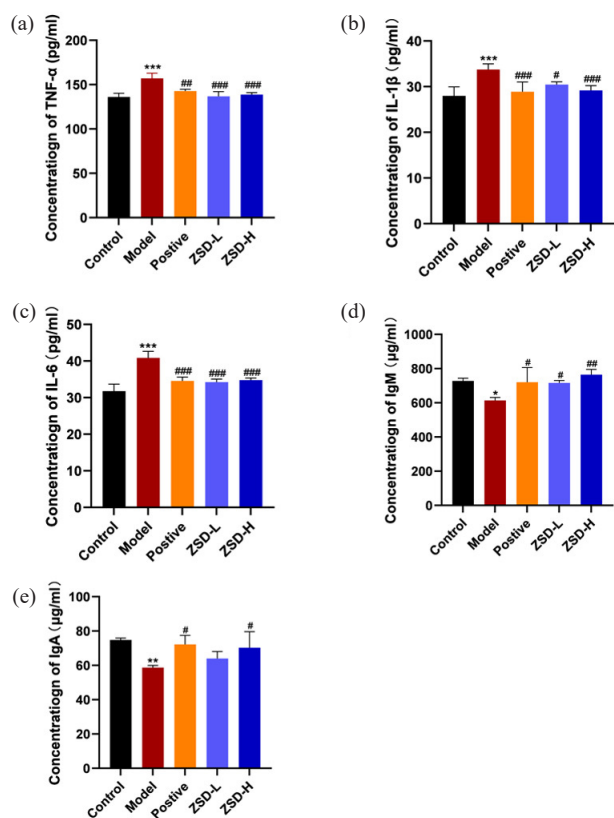


**Figure 3.** The expression of inflammatory factors and immune proteins in the serum of each group of mice, including (a) TNF- $\alpha$ , (b) IL-1 $\beta$ , (c) IL-6, (d) IgM, and (e) IgA. Statistical significance is indicated as follows: \* $P < 0.05$ , \*\* $P < 0.01$ , \*\*\* $P < 0.001$  when compared to the control group; # $P < 0.05$ , ## $P < 0.01$ , ### $P < 0.001$  when compared to the model group.

acquired from both positive and negative ionization modes. The PLS-DA score plot for the positive ion mode, illustrated in Figure 5(a), clearly demonstrates a distinct separation between the control and model groups. This separation signifies the occurrence of metabolic alterations in mice with LPS-induced acute pneumonia. This model's R2Y and Q2 values were 0.982 and 0.872, respectively, suggesting good predictability and fitness. After being treated with ZSD-H, the score plot (Figure 5b) shows that the group separated from the model group to the right side of the y-axis, together with the control group, suggesting the ZSD could modulate the metabolome back to normal to exert the therapeutic effect on acute pneumonia. The permutation test results in Figure 5(c) and (d) show that the calculated R2 and Q2 were lower than the original value, suggesting no overfitness in both PLS-DA models.

The VIP value was calculated to show the importance of the feature's contribution to the sample classifications. The PLS-DA loading plot has been shown in Figure 5(e), in which the point farther away from the origin indicates that the variable contributes more to the classification. The features with VIP  $> 1$  are marked in red, and these points are all located far away from the origin, which are selected as the biomarker candidates. Then, the FC and t-test P values were applied to further filter the biomarkers and observe whether their intensities significantly differed between groups. The volcano plot in Figure 5(f) highlights the features that meet the criteria. Metabolites exhibiting a VIP score exceeding 1, a fold change greater than 1.5, and a P value below 0.05 were selected as potential biomarkers associated with acute pneumonia. Similar results have been depicted in Figure 6(a-d), in which the model was constructed using the data obtained from negative ion mode. Biomarkers obtained were highlighted using above procedures (Figure 6e and 6f).

Chemical structures of the above-selected biomarkers were annotated by database searching in HMDB using its accurate m/z value MS/MS information. The annotation process of LysoPC (16:0/0:0) at RT 17.62 min\_m/z 496.3398 was described as follows. The MS spectrum of

this metabolite has been presented in Figure 7(a). The peak observed at m/z 496.3398 corresponds to the protonated molecule, while the ion at m/z 991.6641 is associated with the  $[2M+H]^+$  species. In Figure 7(b), the fragment ion at m/z 478.3301 is generated through the loss of an  $H_2O$  molecule from the precursor ion, whereas the ion at m/z 313.2746 results from the detachment of the headgroup unit at m/z 184.0731. The fragment ions detected at m/z 104.1082 and m/z 125.0032 are attributed to the  $[(CH_3)_3N(CH_2)_2O^+H]$  moiety from the headgroup and the  $[head\ group-(CH_3)_3N^+H]$  ion, respectively. Based on this spectral data, the compound was tentatively identified as LysoPC (16:0/0:0). A total of 74 serum metabolites were finally identified, and the results have been listed in Table S1. The impact of ZSD on these metabolites was then assessed by comparing the intensities between the ZSD-H group and the model group, and the results showed that 67 of the 74 changed metabolites were reversed-regulated, suggesting the ZSD exerted the therapeutic effect on acute pneumonia through modulating these metabolisms of these compounds.

### 3.5. Network construction and target selection

The CMM-AI-T network was constructed to exhibit the relationship network among the active ingredient and their targets and highlight the core bioactive components of ZSD based on connectivity degree. As shown in Figure 8(a), this CMM-AI-T network contains 511 nodes and 11786 edges. A Venn diagram was employed to intersect the targets linked to the active ingredients of ZSD and those implicated in acute pneumonia (Figure 8b). This analysis revealed a total of 213 common targets, indicating that ZSD has the potential to modulate multiple targets, thereby exerting therapeutic effects on acute pneumonia.

The PPI network of overlapping targets associated with ZSD and acute pneumonia was constructed utilizing the STRING database. As illustrated in Figure 8(c), the PPI network comprises 212 nodes and 3924 edges. The degree of each target was computed, where a higher degree signifies a more pivotal role of the node within the PPI network. The findings revealed that proteins such as AKT1, IL-6, IL-1 $\beta$ , TNF, MYC, PPARG, PTGS2, STAT3, TP53, BCL2, CASP3, EGFR, ESR1, and HIF1A exhibited degree values exceeding 90, underscoring their significant involvement in the network and their potential as therapeutic targets for ZSD in the treatment of acute pneumonia. The detailed information on the nodes in network pharmacology analysis has been listed in Table S2.

### 3.6. Joint pathway analysis

Changes in biomarkers reflect altered metabolic phenotypes and provide us with information to understand the metabolic regulation action of ZSD. Key targets were obtained from network pharmacology analysis to show the potential action of the mechanism of ZSD. The joint pathway analysis was performed by integrating these 74 biomarkers and key targets into the MetaboAnalyst 6.0 software for enrichment analysis, with the results presented in Figure 9. The findings indicate that multiple pathways, such as arachidonic acid metabolism, sphingolipid metabolism, glycerophospholipid metabolism, the PPAR signaling pathway, and the JAK-STAT signaling pathway, were affected during the LPS modeling and subsequent ZSD treatment.

### 3.7. Discussion

Acute pneumonia is predominantly attributable to infections, with its onset primarily associated with the overwhelming proliferation and heightened virulence of pathogenic microorganisms. The common symptoms are high fever, coughing, and difficulty in breathing. ZSD is a typical TCM formula with the medicinal effects of removing heat to promote salivation, tonifying qi, and regulating the stomach. Based on the principles of TCM diagnosis and treatment, ZSD demonstrates therapeutic potential for patients with acute pneumonia during the recovery phase. Specifically, it is beneficial for individuals experiencing high fever, those whose fever has resolved but exhibits lingering symptoms of residual fever, or those suffering from a dual deficiency of qi and yin, characterized by restlessness, thirst, and general debility. However, the precise mechanism underlying its action has yet to be

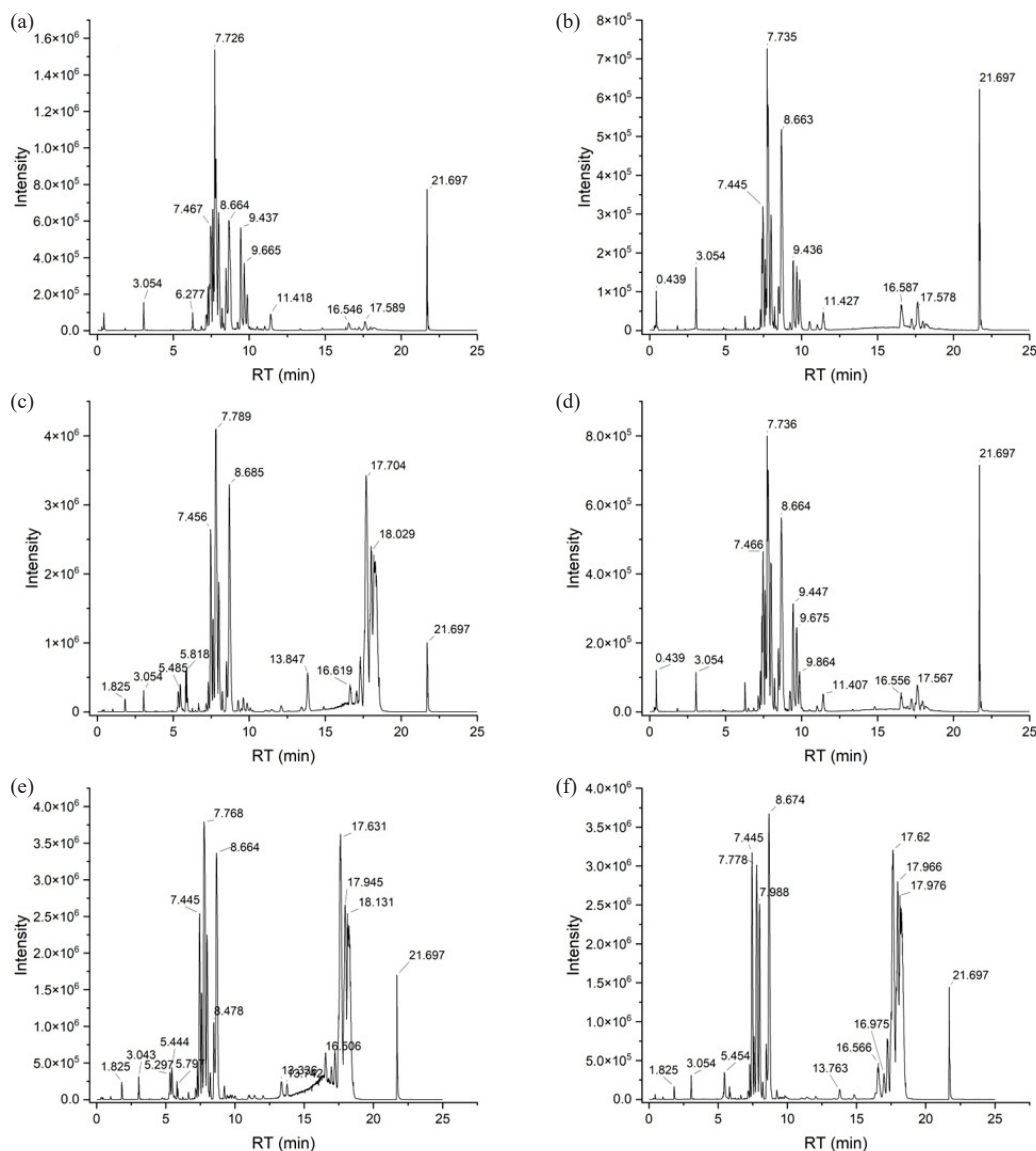


**Figure 4.** BPCs for (a-b) the control, (c-d) model, and (e-f) ZSD-H groups, as acquired in (a, c, and e) negative and (b, d, and f) positive ioniza.

fully elucidated. In this study, we established a mouse model of LPS-induced acute pneumonia and gave ZSD for treatment. ZSD treatment has been shown to mitigate tissue inflammatory cell infiltration, suppress alveolar epithelial cell hyperplasia, and alleviate capillary dilation within the alveolar walls, all of which are characteristic features observed in the model group. Proinflammatory cytokine aggregation has been reported as a mechanism for the pathogenesis of pneumonia [24]. Studies have demonstrated that TNF- $\alpha$ , IL-1 $\beta$ , and IL-6 can influence the central thermoregulatory system, leading to persistent hyperthermia. Among these, IL-1 $\beta$  is particularly notable for its strong proinflammatory activity, as it induces the production of a wide array of proinflammatory mediators, including cytokines and chemokines [25]. IgA plays a pivotal role in the mucosal defense system of the human respiratory tract, while IgM is essential for the body's humoral immune response. In this study, the ZSD treatment groups, in comparison to the model group, exhibited a significant decrease in the expression levels of pro-inflammatory cytokines TNF- $\alpha$ , IL-1 $\beta$ , and IL-6, alongside a notable increase in the expression levels of IgA and IgM. These findings suggested that ZSD possessed therapeutic potential for acute pneumonia by modulating the expression of inflammatory cytokines, mitigating inflammatory responses, and enhancing immune function.

In this study, a total of 74 serum metabolites were identified as potential biomarkers through an LC-MS-based metabolomics approach. Among these, 67 metabolites, primarily comprising lipids and fatty acids, were reversely modulated by ZSD treatment. Compared with the model group, the intensities of lysophosphatidylcholine (LysoPC), sphingomyelin (SM), phosphatidylcholine (PC), and phosphatidylserine (PS) were significantly elevated in the ZSD-H group, while oxidized phosphatidic acid (PA), phosphatidylglycerol (PG), and cardiolipin (CL) were significantly reduced. These metabolites are mainly involved in arachidonic acid metabolism, sphingolipid metabolism, and glycerophospholipid metabolism. PA is the simplest phospholipid that can bond to several organic molecules, such as the combination with phosphate groups to produce LysoPC, PC, PS, PG, etc. [9].

LysoPC is a monoglycerophospholipid involved in various biological functions, including promoting inflammation, oxidative stress, apoptosis induction, and anti-infection effects [26]. LysoPC is primarily generated through the hydrolysis of phosphatidylcholine by phospholipase A2 (PLA2) at the sn-2 position. It undergoes further metabolism and catabolism *via* various enzymatic pathways, producing free fatty acids like arachidonic acid (AA) [27, 28]. These fatty acids are subsequently converted into active proinflammatory mediators, including prostaglandins, thromboxanes, leukotrienes, and

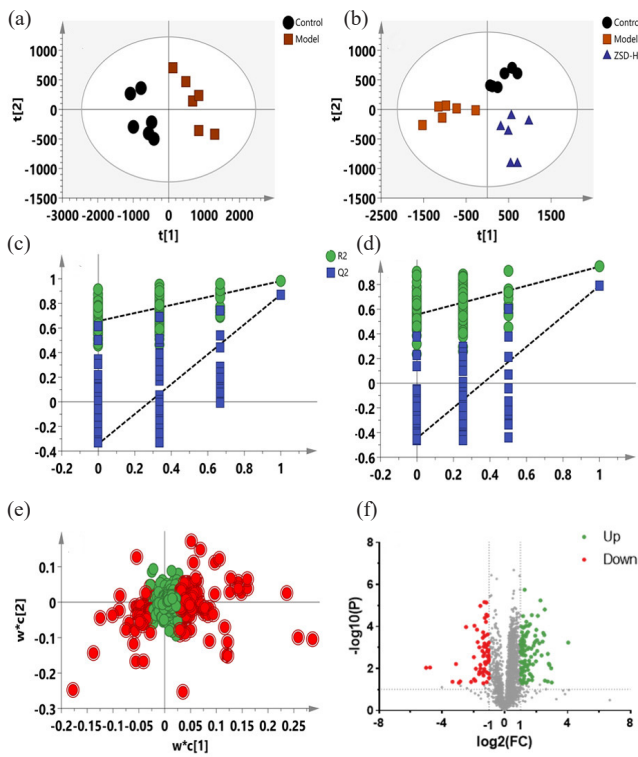


**Figure 5.** PLS-DA score plots (a-b), permutation test plots (c-d), PLS-DA loading plots (e), and volcano plots (f) for the control, model, and ZSD-H groups based on the data from negative ion mode.

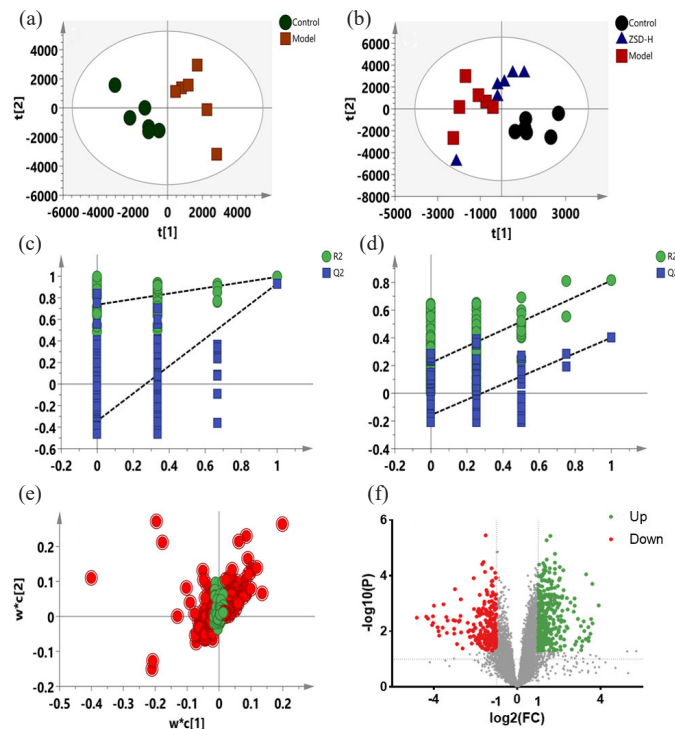


**Figure 6.** PLS-DA score plots (a-b), permutation test plots (c-d), PLS-DA loading plots (e), and volcano plots (f) for the control, model, and ZSD-H groups based on the data from positive ion mode.

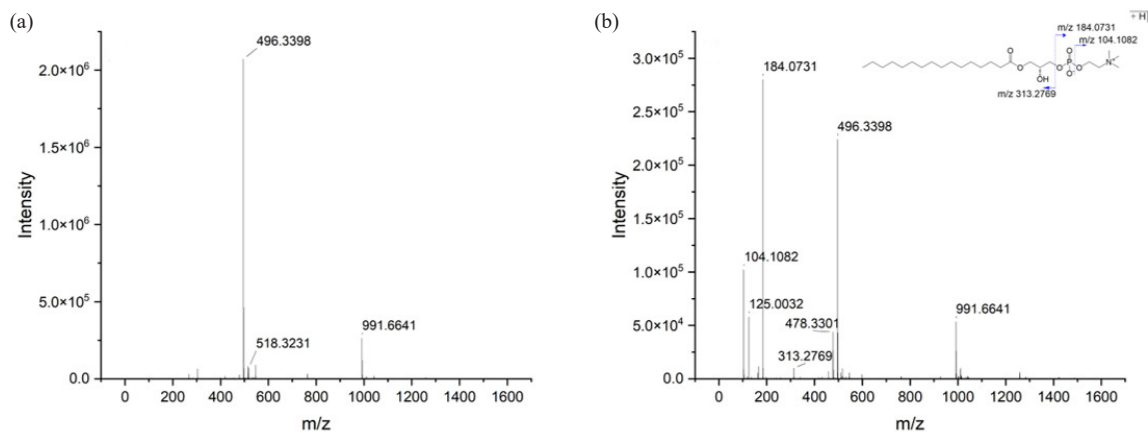


**Figure 7.** (a) MS and (b) MS/MS spectra of LysoPC (16:0/0:0) obtained in positive ion mode.

lipoxins [29]. LysoPC can be converted into lysophosphatidic acid (LysoPA) by autotaxin (ATX), an ectonucleotide pyrophosphatase/phosphodiesterase 2 enzyme with lysophospholipase D activity. As a proinflammatory mediator, ATX represents a promising therapeutic target for potential future treatments of inflammatory diseases [30, 31]. Besides, LysoPC can enhance ATX production by promoting the synthesis of cyclooxygenase-2 and various inflammatory cytokines, which in turn activate multiple signaling pathways involved in oxidative stress and inflammation [32]. In addition, LysoPC can participate in AA metabolism, thereby increasing the production of proinflammatory cytokines in macrophages [33, 34] and promoting the transition of macrophages to proinflammatory M1 phenotype through a G2A-mediated pathway [35].

The result of integrative analysis of metabolomics and network pharmacology showed that the peroxisome proliferator-activated receptor (PPAR) signaling pathway was modulated during ZSD treatment and was intricately associated with inflammatory processes.

It was reported that the LPS stimulation increased Th1 cytokines (e.g., TNF- $\alpha$ , IL-1 $\beta$ , IL-6, IL-12) and decreased the Th2 cytokine IL-10 in macrophages of PPAR $\gamma$ -deficient mice [36]. In research on fatty acid-induced inflammation, LysoPC significantly reduced IL-6, ATF3, and CXCL3 expression triggered by palmitic acid. Studies suggest that LysoPC activates PPAR $\delta$ , a critical pathway through which PPAR $\delta$  exerts its anti-inflammatory effects by reducing cytokine and chemokine expression and release in muscle cells, adipocytes, and other cell types. Thus, PPAR $\delta$  activation protected skeletal muscle from fatty acid-induced inflammatory damage and modulated the anti-inflammatory activity of adipocytes and macrophages, preventing leukocyte recruitment to endothelial cells [37]. Therefore, ZSD may exert a therapeutic effect on acute through the PPAR signaling pathway by increasing the serum concentration of LysoPC.

Sphingolipid metabolism plays a crucial role in regulating inflammatory signaling pathways [38]. The first evidence for the involvement of sphingolipids in lung inflammation is the production

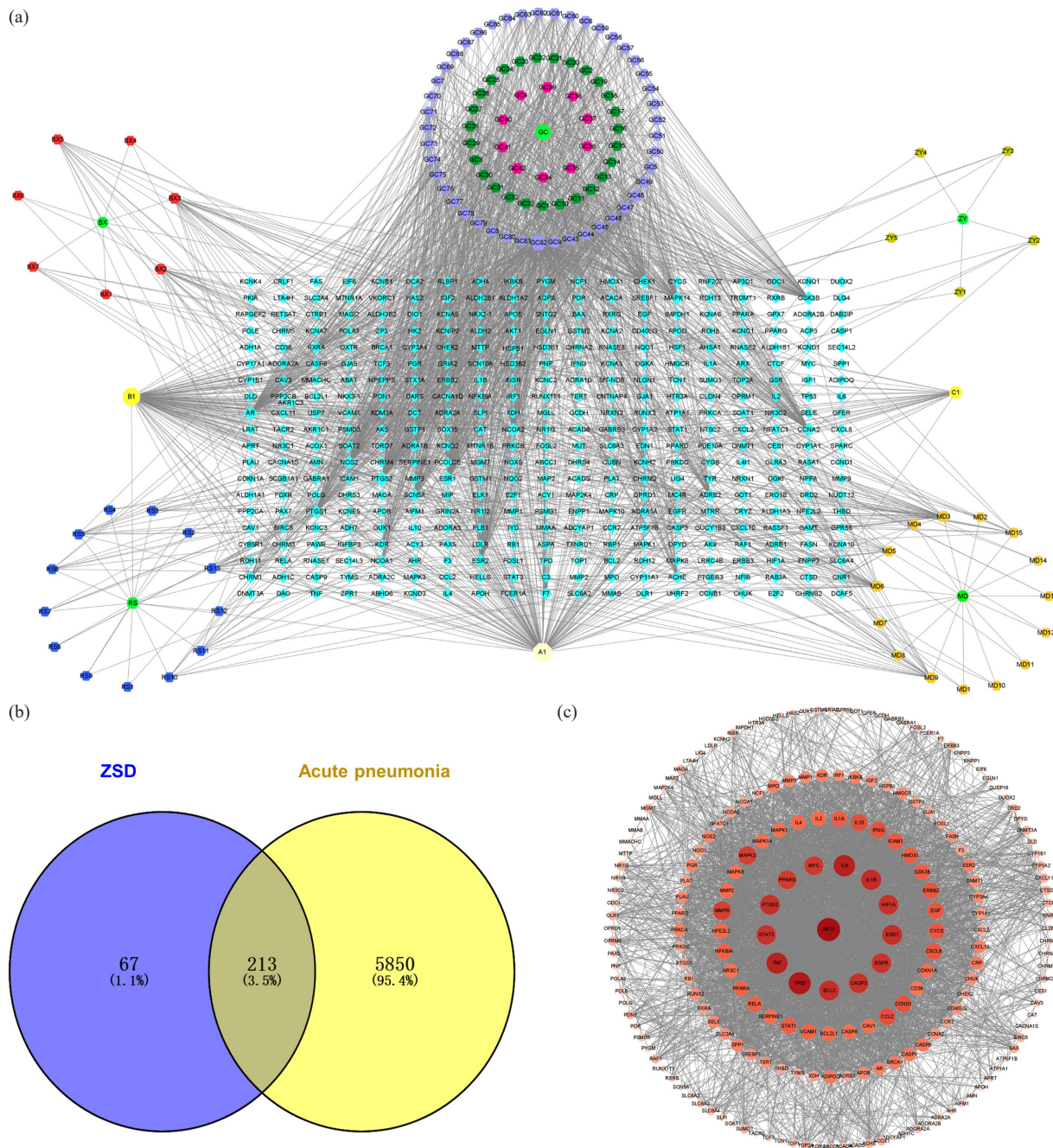


Figure 8. (a) The CMM-active ingredient-target (CMM-AI-T) network, CMM (●), active ingredient (●), target (◆), common ingredients of CMMs (●). (b) The Venn diagram overlap highlighted the potential target of ZSD for treating acute pneumonia. (c) The PPI network was constructed using the selected potential targets.

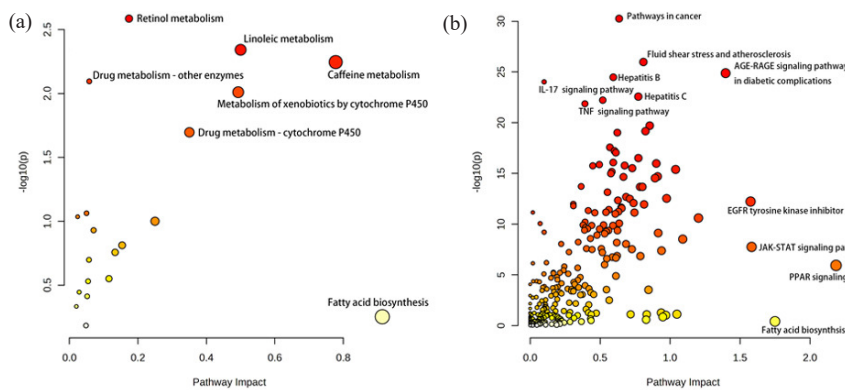


Figure 9. Bubble diagram of joint pathway analysis using the data obtained from (a) negative and (b) positive ion modes.

of autoantibodies against sphingolipids by responsive Mycoplasma pneumonia infection of the lungs [39]. A study demonstrated that sphingolipids were implicated in a range of pathological conditions, such as pulmonary edema, the modulation of inflammatory mediators, and the decline in lung function [40]. Sphingolipid metabolites, particularly sphingolipids, ceramides, and sphingosine-1-phosphate (S1P), were associated with lung inflammation. In the present study, serum SM levels increased significantly after treatment with ZSD, which is consistent with the finding that SM levels significantly decreased in asthmatic patients [41]. Therefore, ZSD may intervene in lung inflammation by affecting SM metabolism.

SM is synthesized by transferring phosphocholine from phosphatidylcholine to ceramide in a reaction catalyzed by SM synthase (SMS). Ceramide is produced by hydrolysis of SM via the sphingomyelinase (SMases), neuroide *de novo*, and recycling pathways. The biosynthetic pathway of SM and ceramide is known as the "SM cycle" [42]. Ceramides are bioactive lipids that play a role in numerous physiological and pathological processes, like inflammation. Ceramide is converted to sphingosine through the action of ceramidases, including human basic phytoceramidase, human basic ceramidase 1, and human basic ceramidase 2. These enzymes use ceramide as a substrate, thereby regulating intracellular levels of sphingosine and S1P [43]. Inhibition of *de novo* ceramide synthesis can mitigate oxidative and nitrosative stress, reduce epithelial cell apoptosis, and alleviate airway inflammation, consequently enhancing respiratory function and ameliorating histopathological abnormalities [44]. Moreover, elevated ceramide production in airway epithelial cells has been observed in experimental asthma models, and alterations in the ceramide content of these cells play a pivotal role in the pathogenesis of inflammatory lung diseases.

The joint pathway analysis highlighted that the JAK-STAT signaling pathway involved disease occurrence and treatment using ZSD. JAK-STAT signaling pathway has been reported to play an essential role in inflammatory and autoimmune diseases. The JAK-STAT signaling pathway serves as a critical mediator of cytokine signaling, activated by various proinflammatory molecules to transduce downstream effects and initiate gene transcription [45]. A study on endogenous ceramide production in cultured fibroblasts treated with SMase demonstrated that ceramide activated STAT1 and STAT3 via tyrosine phosphorylation initiated by JAK2 activation [46]. Research also demonstrated that ceramide stimulated matrix metalloproteinase 9 (MMP-9) production by activating the JAK2-STAT3 pathway, identifying it as a potent inducer of MMP-9 in airway epithelial cells [47]. MMP-9 is a pivotal enzyme involved in the remodeling of the extracellular matrix, responsible for the degradation of elastin, collagen, fibronectin, and other extracellular proteins. It plays a critical role in facilitating the infiltration of inflammatory cells into the airways during inflammatory responses [48]. Furthermore, up-regulated levels of MMP-9 were detected in exhaled breath condensate, bronchoalveolar lavage fluid (BALF), and sputum of patients suffering from asthma and chronic obstructive pulmonary disease (COPD) [49]. Consequently, sphingolipid metabolites have the potential to activate the JAK-STAT signaling pathway, thereby modulating inflammatory responses. This mechanism may represent an additional pathway through which ZSD exerted its therapeutic effects in the management of acute pneumonia.

ZSD could regulate biosynthetic metabolic pathways, such as arachidonic acid and sphingolipid metabolism, to influence the concentrations of related metabolites. The changed metabolites could further exert activities through modulating the signaling pathways, like PPAR and JAK-STAT signaling pathways, to exert a therapeutic effect on acute pneumonia. This study exhibited the comprehensive regulatory role of ZSD in disease treatment, which reflected the characteristics of TCM in terms of multiple components, targets, and pathways.

#### 4. Conclusions

In this study, we investigated the efficacy of ZSD in the treatment of acute pneumonia using an LPS-induced acute pneumonia mouse model. Its potential mechanisms were explored using LC-MS-based metabolomics combined with network pharmacology analysis. Serum biochemical analyses and HE staining showed that ZSD reduced

inflammatory factors and improved lung tissue changes. A total of 74 metabolites were selected in serum as metabolic biomarkers that changed significantly during modeling, 67 of which were reversed-regulated after being treated with ZSD. Network pharmacology analysis highlighted seven proteins that may associated with the efficacy of ZSD on acute pneumonia. Joint pathway analyses suggest that the medicinal efficacy of ZSD may be related to sphingolipid metabolism, AA metabolism, and PPAR and JAK-STAT signaling pathways. Additional research is necessary to validate these findings, which will advance our comprehension of the regulatory mechanisms of ZSD in the context of acute pneumonia. This study lays the groundwork for the prospective application of ZSD in the treatment of acute pneumonia.

#### CRediT authorship contribution statement

**Zhiliang Sun and Haipeng Tang:** Methodology, Software; **Zhiliang Sun:** Writing - Original draft preparation; **Guangzhi Cai and Kejin Xu:** Investigation, Data curation; **Jiyu Gong:** Supervision; **Yang Wang:** Supervision and Writing- Reviewing and Editing.

#### Declaration of competing interest

The authors declare that there is no conflict of interest.

#### Declaration of Generative AI and AI-assisted technologies in the writing process

The authors confirm that there was no use of artificial intelligence (AI)-assisted technology for assisting in the writing or editing of the manuscript and no images were manipulated using AI.

#### Acknowledgment

This study was supported by the China National Traditional Chinese Medicine Standardization Project (Grant No. ZYBZH-Y-JL-25) and the Changchun University of Chinese Medicine (Grant No. 2023JQ05).

#### Supplementary data

Supplementary material to this article can be found online at [https://dx.doi.org/10.25259/AJC\\_192\\_2024](https://dx.doi.org/10.25259/AJC_192_2024).

#### References

- Lin, L., Yan H., Chen J., Xie H., Peng L., Xie T., Zhao X., Wang S., Shan J., 2019. Application of metabolomics in viral pneumonia treatment with traditional Chinese medicine. *Chinese Medicine* 14: 8. <https://doi.org/10.1186/s13020-019-0229-x>
- Kim, S.W., Jee W., Park S.M., Park Y.R., Bae H., Na Y.C., Lee H.G., Kwon S., Jang H.J., 2024. Anti-inflammatory Effect of Symlocos prunifolia Extract in an In Vitro Model of Acute Pneumonia. *Plant Foods for Human Nutrition* 79: 893-900. <https://doi.org/10.1007/s11130-024-01231-5>
- Ding, J., 2017. Clinical Effect of Tanreqing Injection Combined With Ceftriaxone Sodium on Acute Pneumonia. *China Continuing Medical Education* 13: 176-7. <https://doi.org/10.3969/j.issn.1674-9308.2017.13.097>
- Chien, T.-J., 2023. The Holistic Philosophy of Traditional Chinese Medicine and Conflicts With Modern Medicine. *Holistic Nursing Practice* 37: 153-160. <https://doi.org/10.1097/HNP.0000000000000508>
- Yin, Z., Li Y., Yuan Z., Mao Y., Long L., Luo C., 2022. Textual Research on Key Information of Classic Prescription Zhuye Shigaotang. *Chinese Journal of Experimental Traditional Medical Formulae* 13: 176-183. <https://doi.org/10.13422/j.cnki.syfx.20230413>
- Zhao, Y., 2023. Effect of Yinqiao San Combined with Lophatherum and Gypsum Decoction and Antibiotic De-escalation Therapy in the Treatment of Severe Pneumonia. *Medical Journal of Liaoning* 37: 88-90.
- Li, J., 2017. Clinical Study of Using Zhuye Shigao Decoction Combined with Maimendong Decoction in the Treatment of Drug-resistant Community-acquired Pneumonia. *Journal of Sichuan of Traditional Chinese* 35: 81-3. <https://doi.org/CNKI:SUN:SCZY.0.2017-02-032>
- Song, Q., Zhang A.-h., Yan G.-l., Liu L., Wang X.-j., 2017. Technological advances in current metabolomics and its application in traditional Chinese medicine. *RSC Advances* 7: 53516-53524. <https://doi.org/10.1039/c7ra02056b>
- Sun, X., Zhao B., Qu H., Chen S., Hao X., Chen S., Qin Z., Chen G., Fan Y., 2021. Sera and lungs metabolomics reveals key metabolites of resveratrol protecting against PAH in rats. *Biomedicine & Pharmacotherapy* 133: 110910. <https://doi.org/10.1016/j.biopha.2020.110910>

10. Sun, Y., Han Y., Guo W., Xu X., Zhao L., Yang J., Li L., Wang Y., Xu Y., 2024. Multi-omics analysis of lung tissue metabolome and proteome reveals the therapeutic effect of Shegan Mahuang Decoction against asthma in rats. *Journal of Ethnopharmacology* **322**: 117650. <https://doi.org/10.1016/j.jep.2023.117650>
11. Zhao, L., Wang S., Xu X., Guo W., Yang J., Liu Y., Xie S., Piao G., Xu T., Wang Y., Xu Y., 2024. Integrated metabolomics and network pharmacology to reveal the lipid-lowering mechanisms of Qizha Shuangye granules in hyperlipidemic rats. *Journal of the Science of Food and Agriculture* **104**: 3265-3274. <https://doi.org/10.1002/jsfa.13213>
12. Zhang, P., Zhang D., Zhou W., Wang L., Wang B., Zhang T., Li S., 2024. Network pharmacology: towards the artificial intelligence-based precision traditional Chinese medicine. *Briefings in Bioinformatics* **25**: bbad518. <https://doi.org/10.1093/bib/bbad518>
13. Tsugawa, H., Cajka T., Kind T., Ma Y., Higgins B., Ikeda K., Kanazawa M., VanderGheynst J., Fiehn O., Arita M., 2015. MS-DIAL: data-independent MS/MS deconvolution for comprehensive metabolome analysis. *Nature Methods* **12**: 523-6. <https://doi.org/10.1038/nmeth.3393>
14. Zheng, Z., Lei J., Chang J., Yi X., Zhou G., Chen J., 2024. Exploring the Mechanisms of the Huangqin Qingfei Decoction in Pneumonia Treatment for Lipopolysaccharide-Induced Mouse Model: A Network Pharmacology Analysis and Experimental Validation. *Natural Product Communications* **19**: 1-21. <https://doi.org/10.1177/1934578X241239843>
15. Han, Y., Guo W., Li X., Xu X., Yang J., Xie S., Liu Y., Zhang H., Wang Y., Xu Y., 2022. LC-MS-based metabolomics reveals the in vivo effect of Shegan Mahuang Decoction in an OVA-induced rat model of airway hyperresponsiveness. *Molecular Omics* **18**: 957-966. <https://doi.org/10.1039/d2mo00216g>
16. Wishart, D.S., Guo A., Oler E., Wang F., Anjum A., Peters H., Dizon R., Sayeeda Z., Tian S., Lee Brian L., Berjanskii M., Mah R., Yamamoto M., Jovel J., Torres-Calzada C., Hiebert-Giesbrecht M., Liu Vicki W., Varshavi D., Varshavi D., Allen D., Arndt D., Khetarpal N., Sivakumaran A., Harford K., Sanford S., Yee K., Cao X., Budinski Z., Liigand J., Zhang L., Zheng J., Mandal R., Karu N., Dambrova M., Schiöth Helgi B., Greiner R., Gautam V., 2022. HMDB 5.0: the Human Metabolome Database for 2022. *Nucleic Acids Research* **50**: D622-D631. <https://doi.org/10.1093/nar/gkab1062>
17. Pang, Z., Lu Y., Zhou G., Hui F., Xu L., Viau C., Spigelman Aliya F., MacDonald Patrick E., Wishart David S., Li S., Xia J., 2024. MetaboAnalyst 6.0: towards a unified platform for metabolomics data processing, analysis and interpretation. *Nucleic Acids Research* **52**: W398-W406. <https://doi.org/10.1093/nar/gkac253>
18. Ru, J., Li P., Wang J., Zhou W., Li B., Huang C., Li P., Guo Z., Tao W., Yang Y., Xu X., Li Y., Wang Y., Yang L., 2014. TCMSP: a database of systems pharmacology for drug discovery from herbal medicines. *Journal of Cheminformatics* **6**: 13. <https://doi.org/10.1186/1758-2946-6-13>
19. Fang, S., Dong L., Liu L., Guo J., Zhao L., Zhang J., Bu D., Liu X., Huo P., Cao W., Dong Q., Wu J., Zeng X., Wu Y., Zhao Y., 2021. HERB: a high-throughput experiment- and reference-guided database of traditional Chinese medicine. *Nucleic Acids Research* **49**: D1197-D1206. <https://doi.org/10.1093/nar/gkaa1063>
20. The UniProt, C., 2015. UniProt: a hub for protein information. *Nucleic Acids Research* **43**: D204-D212. <https://doi.org/10.1093/nar/gku989>
21. Safran, M., Dalah I., Alexander J., Rosen N., Iny Stein T., Shmoish M., Nativ N., Bahir I., Doniger T., Krug H., Sirota-Madi A., Olender T., Golan Y., Stelzer G., Harel A., Lancet D., 2010. GeneCards Version 3: the human gene integrator. *Database* **2010**: baq020. <https://doi.org/10.1093/database/baq020>
22. Kohl, M., Wiese S., Warscheid B., 2011. Cytoscape: Software for Visualization and Analysis of Biological Networks. *Data Mining in Proteomics: From Standards to Applications*. M. Hamacher, M. Eisenacher and C. Stephan. Totowa, NJ, Humana Press: 291-303.
23. Szklarczyk, D., Gable A.L., Nastou K.C., Lyon D., Kirsch R., Pyysalo S., Doncheva N.T., Legeay M., Fang T., Bork P., Jensen L.J., von Mering C., 2021. The STRING database in 2021: customizable protein-protein networks, and functional characterization of user-uploaded gene/measurement sets. *Nucleic Acids Research* **49**: D605-D612. <https://doi.org/10.1093/nar/gkaa1074>
24. Sun, X., Hou T., Cheung E., Iu T.N.-T., Tam V.W.-H., Chu I.M.-T., Tsang M.S.-M., Chan P.K.-S., Lam C.W.-K., Wong C.-K., 2020. Anti-inflammatory mechanisms of the novel cytokine interleukin-38 in allergic asthma. *Cellular & Molecular Immunology* **17**: 631-646. <https://doi.org/10.1038/s41423-019-0300-7>
25. Wang, Y., Che M., Xin J., Zheng Z., Li J., Zhang S., 2020. The role of IL-1 $\beta$  and TNF- $\alpha$  in intervertebral disc degeneration. *Biomedicine & Pharmacotherapy* **131**: 110660. <https://doi.org/10.1016/j.biopha.2020.110660>
26. Zhang, S.-Y., Dong Y.-Q., Wang P., Zhang X., Yan Y., Sun L., Liu B., Zhang D., Zhang H., Liu H., Kong W., Hu G., Shah Y.M., Gonzalez F.J., Wang X., Jiang C., 2018. Adipocyte-derived Lysophosphatidylcholine Activates Adipocyte and Adipose Tissue Macrophage Nod-Like Receptor Protein 3 Inflammasomes Mediating Homocysteine-Induced Insulin Resistance. *EBioMedicine* **31**: 202-216. <https://doi.org/10.1016/j.ebiom.2018.04.022>
27. Ren, J., Lin J., Yu L., Yan M., 2022. Lysophosphatidylcholine: Potential Target for the Treatment of Chronic Pain. *Journal*. **23**. <https://doi.org/10.3390/jms23158274>
28. Sueajai, J., Sutjarit N., Boonmuen N., Auparakkitanon S., Noumjad N., Suksamram A., Vinayavekhin N., Piyachaturawat P., 2022. Lowering of lysophosphatidylcholines in ovariectomized rats by Curcuma comosa. *PLoS One* **17**: e0268179. <https://doi.org/10.1371/journal.pone.0268179>
29. Hanna, V.S., Hafez E.A.A., 2018. Synopsis of arachidonic acid metabolism: A review. *Journal of Advanced Research* **11**: 23-32. <https://doi.org/10.1016/j.jare.2018.03.005>
30. Gendaszewska-Darmach, E., 2008. Lysophosphatidic acids, cyclic phosphatidic acids and autotaxin as promising targets in therapies of cancer and other diseases. *Acta biochimica Polonica* **55**: 227-240;
31. Shi, W., Peng K., Yu H., Wang Z., Xia S., Xiao S., Tian D., Vallance B.A., Yu Q., 2023. Autotaxin (ATX) inhibits autophagy leading to exaggerated disruption of intestinal epithelial barrier in colitis. *Biochimica et Biophysica Acta (BBA) - Molecular Basis of Disease* **1869**: 166647. <https://doi.org/10.1016/j.bbdis.2023.166647>
32. Yamakawa, T., Ohnaka K., Tanaka S., Utsunomiya H., Kamei J., Kadonosono K., 2008. Cyclooxygenase-2 induction by lysophosphatidylcholine in cultured rat vascular smooth muscle cells: involvement of the p38MAPK pathway. *Biomedical research* **29**: 1-8. <https://doi.org/10.2220/biomedres.29.1>
33. Oestvang, J., Anthonsen M.W., Johansen B., 2011. LysoPC and PAF Trigger Arachidonic Acid Release by Divergent Signaling Mechanisms in Monocytes. *Journal of Lipids* **2011**: 532145. <https://doi.org/10.1155/2011/532145>
34. Olofsson, K.E., Andersson L., Nilsson J., Björkbacka H., 2008. Nanomolar concentrations of lysophosphatidylcholine recruit monocytes and induce pro-inflammatory cytokine production in macrophages. *Biochemical and Biophysical Research Communications* **370**: 348-352. <https://doi.org/10.1016/j.bbrc.2008.03.087>
35. Qin, X., Qiu C., Zhao L., 2014. Lysophosphatidylcholine perpetuates macrophage polarization toward classically activated phenotype in inflammation. *Cellular Immunology* **289**: 185-190. <https://doi.org/10.1016/j.cellimm.2014.04.010>
36. Toobian, D., Ghosh P., Katkar G.D., 2021. Parsing the Role of PPARs in Macrophage Processes. *Frontiers in immunology* **12**: 783780. <https://doi.org/10.3389/fimmu.2021.783780>
37. Klingler, C., Zhao X., Adhikary T., Li J., Xu G., Häring H.-U., Schleicher E., Lehmann R., Weigert C., 2016. Lysophosphatidylcholines activate PPAR $\delta$  and protect human skeletal muscle cells from lipotoxicity. *Biochimica et Biophysica Acta (BBA) - Molecular and Cell Biology of Lipids* **1861**: 1980-1992. <https://doi.org/10.1016/j.bbalip.2016.09.020>
38. Norris, G.H., Blesso C.N., 2017. Dietary and Endogenous Sphingolipid Metabolism in Chronic Inflammation. *Nutrients* **9**: 1180. <https://doi.org/10.3390/nu9111180>
39. Ghidoni, R., Caretti A., Signorelli P., Snider A., 2015. Role of Sphingolipids in the Pathobiology of Lung Inflammation. *Mediators of Inflammation* **2015**: 487508. <https://doi.org/10.1155/2015/487508>
40. Okuro, R.T., Machado M.N., Casquilho N.V., Jardim-Neto A., Roncally-Carvalho A., Atella G.C., Zin W.A., 2018. The role of sphingolipid metabolism disruption on lipopolysaccharide-induced lung injury in mice. *Pulmonary Pharmacology & Therapeutics* **50**: 100-110. <https://doi.org/10.1016/j.pupt.2018.04.008>
41. Guo, C., Sun L., Zhang L., Dong F., Zhang X., Yao L., Chang C., 2021. Serum sphingolipid profile in asthma. *Journal of Leukocyte Biology* **110**: 53-9. <https://doi.org/10.1002/JLB.3MA1120-719R>
42. Taniguchi, M., Okazaki T., 2021. Role of ceramide/sphingomyelin (SM) balance regulated through "SM cycle" in cancer. *Cellular Signalling* **87**: 110119. <https://doi.org/10.1016/j.cellsig.2021.110119>
43. Khan, S.A., Goliwasi K.F., Deshane J.S., 2021. Sphingolipids in Lung Pathology in the Coronavirus Disease Era: A Review of Sphingolipid Involvement in the Pathogenesis of Lung Damage. *Frontiers in Physiology* **12**: 760638. <https://doi.org/10.3389/fphys.2021.760638>
44. Masini, E., Giannini L., Nistri S., Cinci L., Mastroianni R., Xu W., Comhair S.A., Li D., Cuzzocrea S., Matuschak G.M., Salvemini D., 2008. Ceramide: a key signaling molecule in a Guinea pig model of allergic asthmatic response and airway inflammation. *The Journal of Pharmacology and Experimental Therapeutics* **324**: 548-557. <https://doi.org/10.1124/jpet.107.131565>
45. Ezeonwumelu, L.J., Garcia-Vidal E., Ballana E., 2021. JAK-STAT Pathway: A Novel Target to Tackle Viral Infections. *Viruses* **13**: 2379. <https://doi.org/10.3390/v13122379>
46. Mazière, C., Conte M.A., Mazière J.C., 2001. Activation of the JAK/STAT pathway by ceramide in cultured human fibroblasts. *FEBS letters* **507**: 163-8. [https://doi.org/10.1016/s0014-5793\(01\)02977-5](https://doi.org/10.1016/s0014-5793(01)02977-5)
47. Xuan, L., Han F., Gong L., Lv Y., Wan Z., Liu H., Ren L., Yang S., Zhang W., Li T., Tan C., Liu L., 2020. Ceramide induces MMP-9 expression through JAK2/STAT3 pathway in airway epithelium. *Lipids in Health and Disease* **19**: 196. <https://doi.org/10.1186/s12944-020-01373-w>
48. Bruun, C.S., Leifsson P.S., Johansen L.K., Jensen H.E., Nielsen J., Fredholm M., 2012. Expression of matrix metalloproteinase-9 and -12 in porcine lung infections. *Journal of comparative pathology* **146**: 253-7. <https://doi.org/10.1016/j.jcpa.2011.05.005>
49. Dragicevic, S., Kosnik M., Divac Rankov A., Rijavec M., Milosevic K., Korosec P., Skerbinjek Kavalar M., Nikolic A., 2018. The Variants in the 3' Untranslated Region of the Matrix Metalloproteinase 9 Gene as Modulators of Treatment Outcome in Children with Asthma. *Lung* **196**: 297-303. <https://doi.org/10.1007/s00408-018-0113-y>